Langmuir

Article

pubs.acs.org/Langmuir

Silver Nanovoid Arrays for Surface-Enhanced Raman Scattering

Xianzhong Lang,[†,‡] Teng Qiu,*[,†,‡] Yin Yin,[†] Fan Kong,[§] Lifang Si,[†] Qi Hao,[†] and Paul K. Chu*[,‡]

[†]Department of Physics and Key Laboratory of MEMS of the Ministry of Education, Southeast University, Nanjing 211189, P. R. China

[‡]Department of Physics and Materials Science, City University of Hong Kong, Kowloon, Hong Kong, P. R. China

[§]School of Chemistry and Chemical Engineering, Southeast University, Nanjing 211189, P. R. China

Supporting Information

ABSTRACT: Highly ordered silver nanovoid arrays are fabricated on porous anodic alumina membranes to produce robust and cost-efficient surface-enhanced Raman scattering (SERS) substrates. Plasmonic tunability can be accomplished by adjusting the topography with different anode voltages. Evenly distributed plasmonic fields, high average enhancement factor, and excellent ambient stability due to the natural protective layer are some of the unique advantages, and the silver nanovoid arrays are applicable to sensing devices.

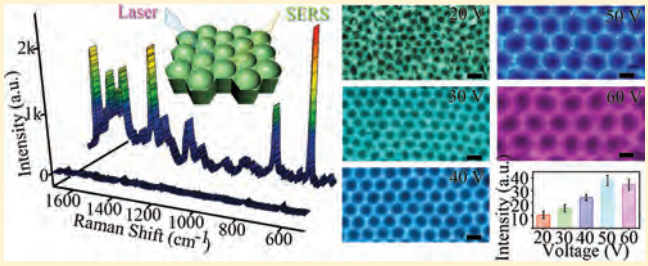

INTRODUCTION

One of the attractive aspects of surface plasmons[1,2] is that subwavelength structures can be used to concentrate and channel light[3] leading to electric field enhancement that can be utilized to manipulate light−matter interactions and boost nonlinear phenomena. In particular, the enhanced localized electromagnetic (EM) field near the metallic surface gives rise surface-enhanced Raman scattering (SERS)[4] and modern nanofabrication and spectroscopic techniques have rendered nondestructive and ultrasensitive characterization down to the single molecular level possible.[5,6] Generally, ordered metal nanostructure arrays that are patterned periodically in two dimensions are referred to as plasmonic crystals and provide a promising platform for SERS sensing.[7,8] Furthermore, plasmonic crystals made of nanoparticle and nanohole/nanovoid arrays of plasmonic materials yield localized surface plasmon resonance which can be tuned by carefully controlling the size, shape, and spacing of the nanostructures.[9,10]

Herein, periodically patterned silver nanovoid arrays are fabricated on porous anodic alumina (PAA) membranes to produce robust and cost-efficient SERS substrates exhibiting significant SERS enhancement. Plasmonic tunability is achieved by altering the topography using different anode voltages. The silver nanovoid arrays on PAA have the following additional advantages: (1) creation of long-range uniform plasmonic structures with centimeter dimensions, (2) excellent stability in air due to natural protection from the barrier layer of PAA, and (3) greater enhancement effects because voids provide larger energy confinement than particles.[11,12]

EXPERIMENTAL SECTION

Synthesis of the Base of PAA Substrates. High-purity aluminum (Al) foils (99.99%, 30 mm × 30 mm × 0.3 mm) were degreased by acetone and electropolished using a mixture of ethanol and perchloric acid with a volume ratio of 5:1 under a constant direct-current (dc) voltage of 15 V for 3 min to further remove surface impurities (Figure 1A). After rinsing in distilled water and drying, the Al foils were anodized separately in a 0.5 M oxalic acid solution at a constant dc voltage of 20 V (30, 40, 50, and 60 V) at 10 °C. In order to obtain an ordered nanopore array, a two-step anodizing process was adopted. The Al foils were first anodized for 2 h followed by immersion into a mixture of chromic acid (1.8 wt %) and phosphoric acid (6 wt %) at 75 °C (1:1 in volume). After 2 h, the alumina layer produced in the first step was removed and the surface of the foil became bright. The anodizing time in the second step was 2 h, and the PAA templates were obtained (Figure 1A,B). The PAA templates were reinforced by copper tape as a protective layer (Figure 1B,C). Finally, the aluminum base was dissolved in a saturated solution of copper sulfate by wet-chemical etching to obtain the PAA substrates with alumina protrusion arrays (Figure 1C,D).

Synthesis of Silver Nanovoids. A silver film about 1 μm thick was deposited on the alumina protrusion arrays in a dc magnetron-sputtering system (Figure 1D,E) (typical magnetron power of about 40 W−410 V and 100 mA). The silver nanovoid arrays were finally obtained by inversing the deposited substrate and dissolving the alumina barrier layer in a 0.5 M sodium hydroxide solution (Figure 1E−G). The silver nanovoid arrays were protected from contamination and oxidation by the barrier layer of PAA with good mechanical and chemical robustness. Hence, storage in a vacuum desiccator was not necessary. To better define the void structure, we define each nanovoid is a part of hollow sphere, where D is the diameter of circular section and H is the spherical void height as shown in Figure 1H.

Instrumentation and Data Acquisition. Scanning electron microscopy (SEM: JEOL JSM-6335F) and atomic force microscopy (AFM: Vecco Nano Scope V) were used to investigate the nanostructures. The AFM probes were composed of a pyramidal tip 14−16 μm long with a radius of curvature of 6 nm connected with a rectangular silicon cantilever with a 30 ± 5 nm aluminum reflex-side coating. The Raman measurements were performed on a Jobin Yvon

Received: April 16, 2012
Revised: May 21, 2012
Published: May 21, 2012

   dx.doi.org/10.1021/la301542n | Langmuir 2012, 28, 8799−8803

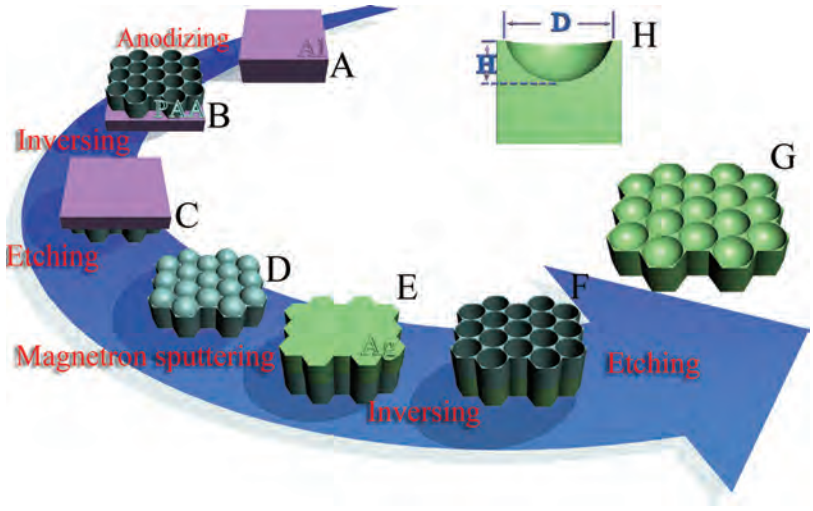

Figure 1. Schematic illustrating the fabrication process for the silver nanovoid arrays: (A) pretreated Al sheets, (B) PAA templates, (C) reinforced and inversed PAA templates, (D) PAA templates with alumina protrusion arrays, (E) silver films which are deposited on the alumina protrusion arrays, (F) silver nanovoid arrays protected by the barrier layer of PAA, (G) silver nanovoid arrays, and (H) void structure.

LabRAM HR800 micro-Raman spectrometer with the 514 nm laser line at room temperature. An area of ~3 μm in diameter was probed by a 50× objective lens (nominal aperture 0.45), and the incident power at the sample was 45 μW. The signal acquisition time was 10 s. In order to evaluate the substrate Raman-enhancing capability, a Rhodamine 6G (R6G) water solution was used. In order to allow molecule adsorption, the substrate was maintained for 30 min in the R6G solution and then taken out and rinsed thoroughly. The acquisition time and laser power were the same for all Raman spectra. The SERS spectra were recorded from multiple sites on the substrate surface to confirm reproducibility. Similar SERS spectral characteristics such as enhancement, position, and relative intensity of the bands were determined from various locations to confirm large area production of uniform geometries.

RESULTS AND DISCUSSION

The large-area SEM image of the representative silver nanovoid array shown in Figure 2A and Figure S1 reveals a honeycomb structure (see the inset of Figure 2A) with each void surrounded by six equivalent adjacent ones and is easily scaled up to contiguous areas cm^2 in size. The high-resolution 3D AFM image in Figure 2B shows that the size of each void is around 100 nm. The cross-sectional geometry of the sample is shown schematically in Figure 2C, and the voids have similar shape and size. By adjusting the anode voltages, a series of silver nanovoid arrays with different sizes can be obtained as shown in Figure 2D–H. The size of each silver nanovoid is consistent with the inverse alumina protrusions on the PAA template (see Figure S2). Moreover, the average D value can be tailored from 60 to 150 nm, and the functional relationship between D and the anode voltage is approximately linear as shown in Figure 2I.

To evaluate the Raman enhancing capability of the silver nanovoids, an aqueous solution (1.0×10^{-5} M) of R6G is used on the substrate. Figure 3A shows the typical Raman spectrum of the R6G solution obtained on the silver nanovoids (anode voltage = 40 V) versus that acquired on the flat aluminum substrate with the same thickness silver coating excited at 514.5 nm. In the range between 500 and 1700 cm^{-1}, many salient peaks emerge. The more prominent ones at 1510, 1537, 1574, and 1649 cm^{-1} can be assigned to the totally symmetric modes of in-plane C–C stretching vibration. In contrast, the normal Raman signature of 1.0×10^{-2} M R6G corresponding to the

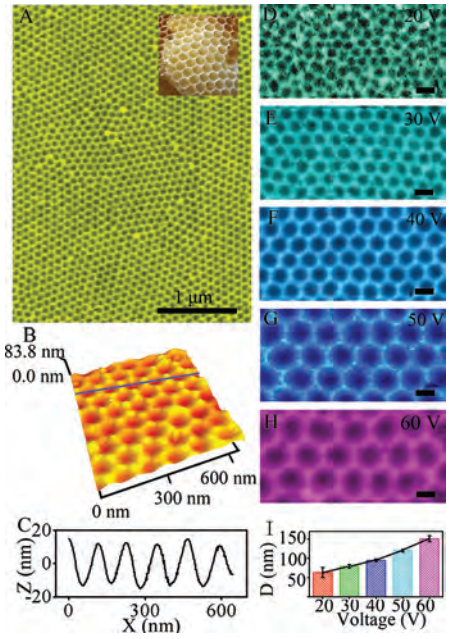

Figure 2. (A) Representative large-area SEM image of the silver nanovoid array. The inset in (A) shows a honeycomb. (B) 3D AFM image acquired from a representative silver nanovoid array. (C) Cross-section analysis along the blue line in (B). A series of SEM images acquired from the silver nanovoid arrays at different voltages of (D) 20, (E) 30, (F) 40, (G) 50, and (H) 60 V. The scale bar is 100 nm. (I) D as a function of voltage. The solid line is a guide to the eye.

silver-coated flat aluminum substrate is only barely recognizable. The empirical enhancement factor is estimated to be larger than 3×10^4 by comparing ratios of the average SERS peak intensity (at 1649 cm^{-1}) of R6G to the corresponding average unenhanced signals. The performance of the same SERS-active substrate in the detection of R6G is illustrated in Figure 3B. The standard error obtained by analyzing 10 Raman spectra of 1.0×10^{-5} M R6G measured at 10 different locations on a typical SERS-active substrate shows less than 9% error for the most intense Raman spectra.

dx.doi.org/10.1021/la301542n | Langmuir 2012, 28, 8799–8803

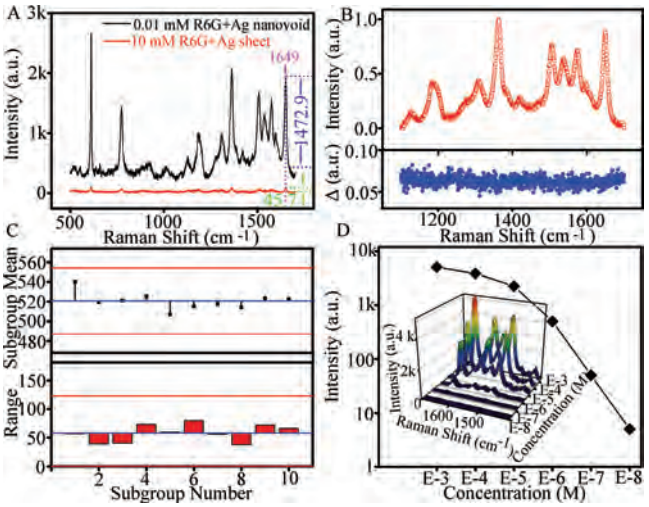

Figure 3. (A) Comparison of Raman spectral characteristics of 10^{-5} M R6G adsorbed on the flat silver sheet and silver nanovoid array. (B) Normalized mean SERS signal Raman spectrum of 10^{-6} M of R6G averaged over 10 spectra measured at 10 random locations of single SERS-active substrate. Their standard error (Δ) is shown below. (C) Statistical quality control chart traces different batches of silver nanoviods: x-bar chart (above) and range chart (below). (D) Average SERS signal at 1649 cm^{-1} as a function of the R6G molecular concentration on a logarithmic scale. Solid line is a guide to the eye.

The repeatability of different production batches is the key to realize mass production and commercial applications of the SERS substrates. However, it is not always possible to inspect every product and aspect of the production process all the time. The challenge is to design ways to maximize the ability to monitor the quality of the SERS substrates produced. One way to ensure a quality product is to build quality into the process. Statistical quality control is used to describe the set of statistical tools used by quality control professionals. The most commonly used tool for monitoring the production process is a quality control chart and different types of quality control charts are used to monitor different aspects of the production process. The mean or x-bar chart measures the central tendency of the process, whereas the range chart measures the dispersion or variance of the process. Every control chart has a center line, an upper control limit, and a lower control limit. The center line of the control chart is the mean of the quality characteristic being measured. The upper control limit is the maximum acceptable variation from the mean for a process that is in a state of control. Similarly, the lower control limit is the minimum acceptable variation from the mean for a process that is in a state of control. The upper and lower control limits on a control chart are usually set at ±3 standard deviations from the mean. Herein, the statistical quality control is introduced into the process to monitor the quality of silver nanovoid arrays. Figure 3C shows the typical quality control chart for silver nanovoids under 40 V inspecting the SERS intensity of 1.0×10^{-6} M R6G at 1649 cm^{-1}. It graphically documents the analytical performance of the system, and the platform construction is described in detail in the Supporting Information. In the x-bar chart, the center line, upper control limit, and lower control limit are 520.6, 554.0, and 487.1, respectively. In the range chart, the center line, upper control limit, and lower control limit are 58.0, 122.7, and 0, respectively. All the results fall inside the control limits, indicating that the discrepancy is within the acceptable level. In addition, small values of the range and standard deviation in Table 1 indicate that the data are closely clustered around the mean. The good repeatability can be attributed to the convenient and well-understood preparation method as well as favorable ordered configuration of the silver nanovoid arrays. Hence, the silver nanovoid arrays can be readily mass produced whereas it tends to be a challenge for other traditional production processes.

Table 1. Statistical Data for the Quality Control Chart

bin	mean	range	std dev
1	540.1	56.5	26.1
2	519.4	39.1	14.6
3	521.2	40.6	17.9
4	525.4	72.9	29.4
5	506.7	59.8	24.3
6	515.0	79.4	31.3
7	517.6	56.0	21.4
8	514.3	37.5	16.2
9	523.5	72.3	26.9
10	522.5	66.1	24.0

Solutions of R6G with different concentrations have been used to study the SERS dynamic range of these SERS substrates. Figure 3D shows the recorded Raman intensity at 1649 cm^{-1} as a function of the molar concentration on a logarithmic scale. The linear correlation from 1.0×10^{-8} to 1.0×10^{-6} M with a proportionality constant of unity suggests that the number of adsorption sites with high Raman enhancement is large enough to accommodate a considerable range of sample concentrations. A nonlinear dependence emerges for concentration above 1.0×10^{-6} M, suggesting that adsorption of R6G onto sites with high enhancement becomes saturated beyond this level as multilayers of R6G molecules accumulate on the substrate surface. In addition, the silver nanovoid arrays show excellent stability in air due to natural protection from the barrier layer of PAA (see Figure S3). In conjunction with the robust enhancement factor obtained across the entire substrate, the broad dynamic range and excellent stability facilitate the use of SERS in chemical/biological sensing applications with high sensitivity.

Resonant light absorption by void plasmons is accompanied by high local-field enhancement[15] to trigger the SERS effects. Since the absorption and local-field properties of these types of nanovoid structures can be effectively tailored by varying the diameter of the voids, the amplification factors can be actively tuned and optimized. As a representative application, we examine the native DNA base adenine. Adenine is chosen because it does not have any appreciable one-photon absorption at the excitation wavelength and so has a very low fluorescence background and minimal interference in the SERS measurement. Moreover, adenine has large potential in genetics studies and also been investigated as a biological molecular probe.[16] The typical SERS spectrum of aqueous 1.0×10^{-5} M adenine are depicted in Figure 4A. The laser power is reduced to 0.02 mW to avoid photodecomposition of the sample. The SERS spectrum of adenine in Figure 4A is consistent with previous data[17] showing a characteristic Raman line at 723 and 1330 cm^{-1} that correspond to the purine ring breathing mode and CN stretching mode, respectively.

The finite-difference time-domain method is adopted to calculate the local EM fields of the void structure. A typical

dx.doi.org/10.1021/la301542n | Langmuir 2012, 28, 8799−8803

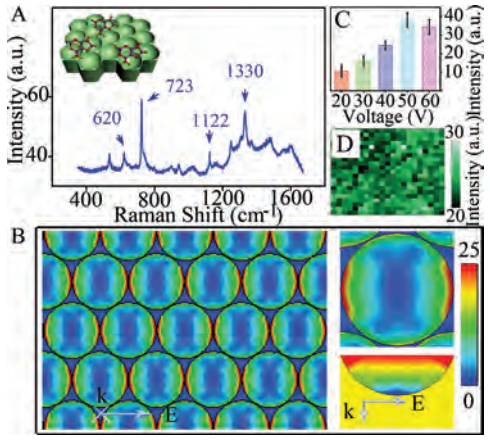

Figure 4. (A) SERS spectrum of aqueous 10^{-5} M adenine. (B) Typical simulated EM-field distribution maps of the silver nanovoid array. The 25-fold enhancement in the EM field does not represent the maximum electric field strength but is artificially set to provide better intuitive models of the EM field. (C) SERS signal at 1330 cm^{-1} as a function of anode voltages. (D) Typical SERS map (63.0 × 63.0 μm^2) obtained from the silver nanovoid array (40 V).

planar and cross-sectional view of the calculated radial EM field components of the silver nanovoid array (40 V) is displayed in Figure 4B. The silver nanovoid array is approximated by the fundamental nanostructure unit composed of seven hexagonally arranged voids using dimensional parameters D and H shown in Figure 1H equal to the mean values of the samples produced experimentally. The radiation at 514 nm is assumed to be normal to the sample surface. Cleary, the maximum localized surface EM field appears near the boundary of the adjacent nanovoids. Since voids embedded in metal films possess additional rim plasmon modes that selectively couple with void plasmons to produce bonding and antibonding hybridized states with significant field enhancements,[18] our calculation shows that these localized resonant plasmon modes are able to produce maximum local enhancement as large as 10^8 for the Raman signal from molecules adsorbed at these boundary of adjacent nanovoids. This exceeds the average over the entire silver nanovoid surface area by several orders of magnitude because most of the optical excitations are localized in these hot spots.[19]

To optimize the amplification factors and evaluate the dependence of the Raman-enhancing capability of the silver nanovoid arrays on different size (see Figure 2D−H), an aqueous 1.0×10^{-5} M adenine is used. Common SERS spectral characteristics such as the position and relative intensity of the bands are determined from multiple and randomly chosen sites on the substrate surface to improve data reliability using the same acquisition time and laser power. Figure 3C shows the SERS peak intensity (at 1330 cm^{-1}) versus anode voltages illustrating the different enhancement efficiency. The Raman enhancement observed from the sample in Figure 2G is larger than that from the others, and the strong enhancement can be attributed to the fact that the nanovoid array is assembled based on a favorable void configuration and highly ordered arrangement,[20] demonstrating good correlation between experiments and theory (see Table 2).

In order to evaluate the reliability of the SERS signals and homogeneity of the silver nanovoid arrays, 2D point-by-point SERS mapping of adenine is performed. Figure 4D displays a typical SERS map of the silver nanovoid array (40 V), and

Table 2. Calculated Data of the Maximum Local Electric Field for Silver Nanovoid Arrays under Different V_{PAA}

voltage (V)	20	30	40	50	60
$\|E_{max}\|$ (V/m)	67.3	71.5	100.7	121.1	107.9

excellent uniformity over a large area of 63.0 × 63.0 μm^2 is achieved by measuring 441 points at a regular scanning step of 3.0 μm. The relative SERS peak intensity of the spots is centered in a narrow range, and the spot-to-spot relative standard deviation is 10%. This indicates that the substrate homogeneity is quite good, and strict control of the preparation conditions can ensure good reproducibility among different sample batches.

CONCLUSION

Silver nanovoid arrays fabricated on PAA membranes are demonstrated to be excellent SERS substrates. The cost-effective spherical nanovoids which can be produced conveniently in mass quantity offer broad spectral tuning of the plasmon modes. Unlike the conventional way to generate hot spots in the gap between two closed nanostructures, the nanovoid arrays introduce hot spots located on the metal surface near the boundary of adjacent nanovoids, and hence, they are more capable of exciting dipoles in the deposited molecules. Moreover, the barrier layer of PAA protects the Raman-enhancing functional layer from contamination and oxidation thereby significantly expanding the applications of SERS to materials and life sciences, food safety, drugs, explosives, and environmental pollution.

ASSOCIATED CONTENT

Supporting Information

A large-area SEM image acquired from a typical silver nanovoid under 40 V, a typical cross-section SEM image acquired from the base of PAA membranes, the recorded average Raman intensity as a function of the storage time, SERS enhancement factor calculation, and statistical quality control. This material is available free of charge via the Internet at http://pubs.acs.org.

AUTHOR INFORMATION

Corresponding Author

*E-mail: tqiu@seu.edu.cn (T.Q.); paul.chu@cityu.edu.hk (P.K.C.).

Notes

The authors declare no competing financial interest.

ACKNOWLEDGMENTS

This work was jointly supported by the National Natural Science Foundation of China under Grant No. 51071045, the Program for New Century Excellent Talents in University of Ministry of Eduction of China under Grant No. NCET-11-0096, Southeast University, Research and Innovation Project for College Graduates of Jiangsu Province No. CXLX_0095, and Hong Kong Research Grants Council (RGC) General Research Funds (GRF) CityU 112510. The finite-difference time-domain simulations are performed at Southeast University.

REFERENCES

(1) Zenneck, J. Über die Fortpflanzung ebener elektromagnetischer Wellen längs einer ebenen Leiterfläche und ihre Beziehung zur drahtlosen Telegraphie. *Ann. Phys.* **1907**, *328*, 846−866.

(2) Ritchie, R. H. Plasma Losses by Fast Electrons in Thin Films. *Phys. Rev.* **1957**, *106*, 874−881.
(3) Barnes, W. L.; Dereux, A.; Ebbesen, T. W. Surface plasmon subwavelength optics. *Nature* **2003**, *424*, 824−830.
(4) Fleischmann, M.; Hendra, P. J.; McQuillan, A. J. Raman spectra of pyridine adsorbed at a silver electrode. *Chem. Phys. Lett.* **1974**, *26*, 163−166.
(5) Nie, S. M.; Emery, S. R. Probing single molecules and single nanoparticles by surface-enhanced Raman scattering. *Science* **1997**, *275*, 1102−1106.
(6) Kneipp, K.; Wang, Y.; Kneipp, H.; Perelman, L. T.; Itzkan, I.; Dasari, R.; Feld, M. S. Single molecule detection using surface-enhanced Raman scattering (SERS). *Phys. Rev. Lett.* **1997**, *78*, 1667−1670.
(7) Gunnarsson, L.; Bjerneld, E. J.; Xu, H.; Petronis, S.; Kasemo, B.; Kall, M. Interparticle coupling effects in nanofabricated substrates for surface-enhanced Raman scattering. *Appl. Phys. Lett.* **2001**, *78*, 802−804.
(8) Qiu, T.; Wu, X. L.; Shen, J. C.; Chu, P. K. Silver nanocrystal superlattice coating for molecular sensing by surface-enhanced Raman spectroscopy. *Appl. Phys. Lett.* **2006**, *89*, 131914.
(9) Lu, Y.; Liu, G. L.; Lee, L. P. High-density silver nanoparticle film with temperature-controllable interparticle spacing for a tunable surface enhanced Raman scattering substrate. *Nano Lett.* **2005**, *5*, 5−9.
(10) Lang, X. Z.; Qiu, T.; Zhang, W. J.; Yin, Y.; Chu, P. K. Tunable Silver Nanocap Superlattice Arrays for Surface-Enhanced Raman Scattering. *J. Phys. Chem. C* **2011**, *115*, 24328−24333.
(11) Coyle, S.; Netti, M. C.; Baumberg, J. J.; Ghanem, M. A.; Birkin, P. R.; Bartlett, P. N.; Whittaker, D. M. Confined plasmons in metallic nanocavities. *Phys. Rev. Lett.* **2001**, *87*, 176801.
(12) Baumberg, J. J.; Kelf, T. A.; Sugawara, Y.; Cintra, S.; Abdelsalam, M. E.; Bartlett, P. N.; Russell, A. E. Angle-resolved surface-enhanced Raman scattering on metallic nanostructured plasmonic crystals. *Nano Lett.* **2005**, *5*, 2262−2267.
(13) O'Sullivan, J. P.; Wood, G. C. The Morphology and Mechanism of Formation of Porous Anodic Films on Aluminium. *Proc. R. Soc. London, Ser. A* **1970**, *317*, 511−543.
(14) Shingubara, S.; Okino, O.; Sayama, Y.; Sakaue, H.; Takahagi, T. Ordered two-dimensional nanowire array formation using self-organized nanoholes of anodically oxidized aluminum. *Jpn. J. Appl. Phys., Part 1* **1997**, *36*, 7791−7795.
(15) Teperik, T. V.; Popov, V. V.; de Abajo, F. J. G. Void plasmons and total absorption of light in nanoporous metallic films. *Phys. Rev. B* **2005**, *71*, 085408.
(16) Kneipp, K.; Kneipp, H.; Kartha, V. B.; Manoharan, R.; Deinum, G.; Itzkan, I.; Dasari, R. R.; Feld, M. S. Detection and identification of a single DNA base molecule using surface-enhanced Raman scattering (SERS). *Phys. Rev. E* **1998**, *57*, R6281−R6284.
(17) Giese, B.; McNaughton, D. Surface-enhanced Raman spectroscopic and density functional theory study of adenine adsorption to silver surfaces. *J. Phys. Chem. B* **2002**, *106*, 101−112.
(18) Cole, R. M.; Baumberg, J. J.; Garcia de Abajo, F. J.; Mahajan, S.; Abdelsalam, M.; Bartlett, P. N. Understanding plasmons in nanoscale voids. *Nano Lett.* **2007**, *7*, 2094−2100.
(19) Kim, W.; Safonov, V. P.; Shalaev, V. M.; Armstrong, R. L. Fractals in microcavities: Giant coupled, multiplicative enhancement of optical responses. *Phys. Rev. Lett.* **1999**, *82*, 4811−4814.
(20) Qiu, T.; Jiang, J. A.; Zhang, W. J.; Lang, X. Z.; Yu, X. Q.; Chu, P. K. High-Sensitivity and Stable Cellular Fluorescence Imaging by Patterned Silver Nanocap Arrays. *ACS Appl. Mater. Interfaces* **2010**, *2*, 2465−2470.

SUPPORTING INFORMATION

Silver nanovoid arrays for surface-enhanced Raman scattering

Xianzhong Lang, [†,‡] Teng Qiu, *[,†,‡] Yin Yin, [†] Fan Kong, [§] Lifang Si, [†] Qi Hao [†] and Paul K. Chu, *[,‡]

[†]Department of Physics and Key Laboratory of MEMS of the Ministry of Education, Southeast University, Nanjing 211189, P. R. China
[‡]Department of Physics and Materials Science, City University of Hong Kong, Kowloon, Hong Kong, P. R. China
[§]School of Chemistry and Chemical Engineering, Southeast University, Nanjing 211189, P. R. China

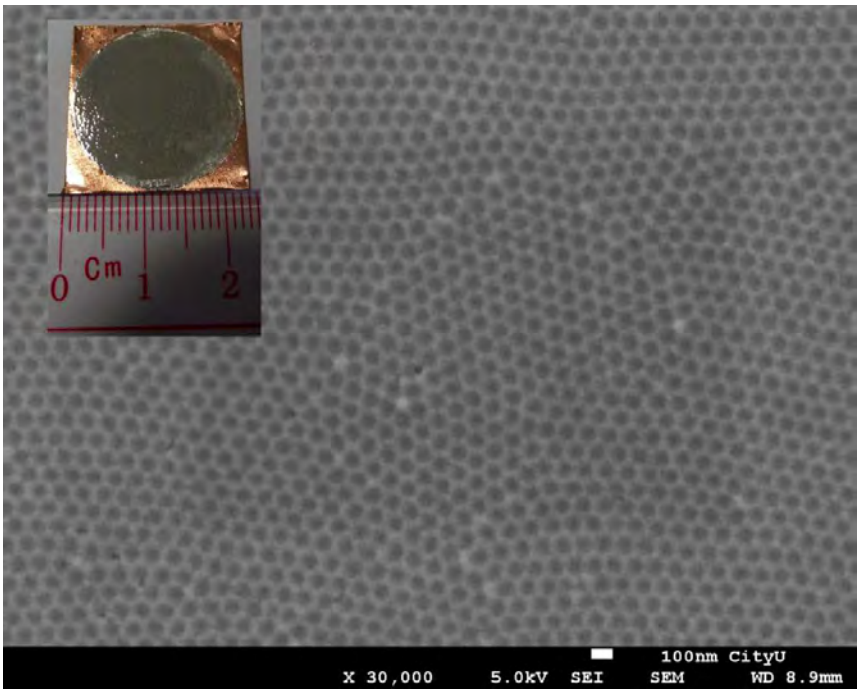

Figure S1. A large-area SEM image acquired from a typical silver nanovoid under 40 V. The inset is an optical photograph of a 2 cm diameter wafer.

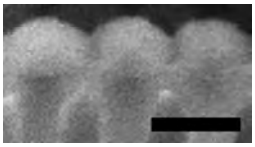

Figure S2. A typical cross-section SEM image acquired from the base of PAA membranes. The scale bar is 100 nm.

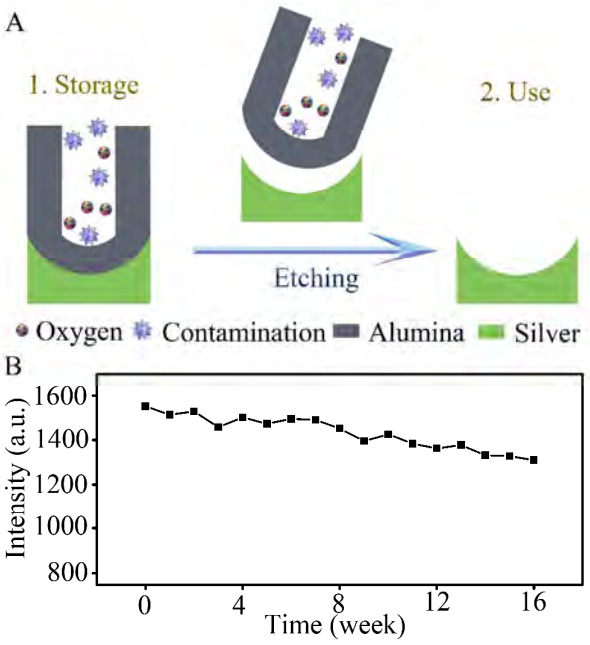

Figure S3. (A) Silver nanovoid arrays are protected from contamination and oxidation by the barrier layer of PAA. (B) Recorded average Raman intensity as a function of the storage time. The small intensity attenuation curve suggests that silver nanovoid arrays have excellent stability in air due to intrinsic protection rendered by the alumina barrier layer.

SERS Enhancement Factor (EF) Calculation

1. Empirical EF (EEF) Calculation

The SERS EEF is estimated by comparing the ratios of the average SERS peak intensity at 1649 cm^{-1} of the probe molecules to the corresponding average unenhanced signals contributed by a surface-adsorbed molecule according to the following equation:

$$EEF = \frac{I_{SERS} / N_{SERS}}{I_{Raman} / N_{Raman}},$$

where I_{SERS} and I_{Raman} represent the Raman intensities for the probe molecules on substrate surface, respectively and N_{SERS} and N_{Raman} represent the numbers of the corresponding molecules that effectively excited by the laser. The experimental conditions such as the laser wavelength, laser power, microscope objective, spot size, spectrometer, and measurement conditions on the substrate are identical in all cases.

2. Theoretical EF (TEF) Calculation

The SERS TEF is estimated by a simplified approximation according to the following equation:

$$TEF = \frac{E_{loc}^4}{E_0^4},$$

where E_{loc} is the location electric-field intensity, and E_0 is the electric-field intensity associated with the incident plane wave.

Statistical quality control

Considering that it is not always possible to inspect every product and every aspect of the production process at all times, statistical quality control is introduced to the process to maximize the ability to monitor the quality of SERS substrates produced. Here, we randomly take ten samples with five observations to inspect the SERS intensity at 1649 cm^{-1} from fifty samples in different batches.

1. x-Bar Charts

An x-bar char is used to monitor changes in the mean of a process. To compute the mean, we sum all the observations and divide by the total number of observations in the same sample. The equation for computing the mean is

$$\bar{x} = \frac{\sum_{i=1}^{n} x_i}{n},$$

where $\bar{x}$, x_i and n are the mean, observation i (i = 1, . . . , n) and number of observations.

Another measure of the variation is the standard deviation (σ). The equation for computing the standard deviation is

$$\sigma = \sqrt{\frac{\sum_{i=1}^{n}\left(x_i - \bar{x}\right)^2}{n-1}}.$$

To construct a mean chart we first construct the center line of the chart. Each sample has its own mean ($\bar{x}_i$). The center line (CL) of the chart is then computed as the mean of all sample means, where N is the number of samples:

$$CL = \frac{\sum_{i=1}^{N}\bar{x}_i}{N}.$$

To construct the upper and lower control limits of the chart, we use the following formulas:

$$UCL = CL + A_2\frac{\sum_{i=1}^{N}R_i}{N},$$

$$LCL = CL - A_2\frac{\sum_{i=1}^{N}R_i}{N},$$

where A_2=0.5768, is a factor that includes three standard deviations of ranges and is dependent on the sample size being considered.

2. Range (R) Charts

R charts constitute another type of control charts to monitor the variability of the process. The range is simply the difference between the largest and smallest values in the same sample:

$$R = x_{max} - x_{min},$$

where x_{max} and x_{min} are the largest and smallest values in the same sample.

The method to develop and use R charts is the same as that for the x-bar charts. The center line of the control chart is the average range and the upper and lower control limits are computed as follows:

$$CL = \frac{\sum_{i=1}^{N} R_i}{N},$$

$$UCL = D_4 CL,$$

$$LCL = D_3 CL,$$

where $D_4 = 2.115$ and $D_3 = 0$.